A 0.5-3GHz Receiver with a Parallel Preselect Filter Achieving 120dB/dec Channel Selectivity and +28dBm Out-of-Band IIP3

Montazerolghaem, M. A.; de Vreede, Leo C. N. ; Babaie, Masoud

A 0.5-3GHz Receiver with a Parallel Preselect Filter Achieving 120dB/dec Channel Selectivity and +28dBm Out-of-Band IIP3

M. A. Montazerolghaem, Leo C. N. de Vreede, and Masoud Babaie

Delft University of Technology, the Netherlands

Recent sub-6GHz receivers (RXs) attempted to realize RF channel selection at the RX input for suppressing large close-in blockers. Although mixer-first RXs can achieve sharp RF filtering and good out-of-band (OOB) linearity, they suffer from large noise figure (NF) and high LO leakage [1][2]. Alternatively, [3]-[5] exploited an N-path notch filter around an LNTA to simultaneously achieve low NF and a moderate channel selection at the RX input. However, their OOB IIP_3 and blocker 1dB compression point (B_{1dB}) are at least 10dB worse than the mixer-first RXs. This paper proposes an LNTA-based RX that shows a similar OOB linearity as prior art mixer-first RXs without sacrificing NF. This is achieved by (1) adding a parallel preselect filter at the RX input to improve the RF selectivity and achieve +6dBm B_{1dB}; (2) proposing third-order RF and baseband filters to attenuate close-in blockers by a 120dB/dec roll-off; (3) introducing a feedback network to reduce the in-band (IB) gain fluctuations to <0.5dB.

Fig.1(a) shows a simplified block diagram of prior art LNTA-based RXs [3]-[5], where a notch filter (Z_N) is placed across the LNTA to provide RF selectivity through Miller theorem, while passive mixers and transimpedance amplifiers (TIAs) downconvert and further filter the input signal. However, when Z_N is replaced with an ideal 3rd-order bandstop filter, the simulated roll-offs of the RX input voltage gain (G_{IN}) and input impedance (Z_{IN}) are much smaller than the ideal 60dB/dec (see Fig.1(c)-(e)). Note that the LNTA's effective load (Z_L) and its open-loop gain ($G_M Z_L$) drop by 20dB/dec at OOB frequencies due to the TIAs' low-pass input impedance and the transparency of passive mixers. Hence, the desired Miller effect at the RX input is corrupted by Z_N interaction with the LNTA's open-loop gain variations at OOB frequencies, degrading the filtering shape and slope.

To resolve that, as shown in Fig.1(b), a preselect filter (PF) consisting of a transconductance stage ($G_{M,P}$) and bandstop filter (Z_N) is added in *parallel* with the RX chain. The LNTA is also exempted from the RF filtering task by removing its notch filter. The PF shunts the blocker current to ground and realizes an RF selectivity directly at the RX input, thus relaxing LNTA linearity requirements. Besides, since no consecutive stages load the PF, its output loading is now constant over frequency, and the Miller shunt equivalent is only defined by Z_N. Hence, by using the same Z_N in this structure, G_{IN} now sharply drops by the ideal 60dB/dec slope and immediately reaches its far-out value, significantly improving OOB IIP_3 and B_{1dB} (see Fig.1(c)-(e)). Moreover, the PF in the absence of large blockers can be turned off to reduce RX power consumption and NF.

To realize Z_N with tunable filters, we propose to employ a 3rd-order high-pass filter and translate its impedance to RF by using the transparency of the passive mixers, as shown in Fig.2. The ground ports of the inductors driven by 180° out-of-phase clocks (i.e., φ_i and $\varphi_{i+M/2}$ where i=1…M/2) are then connected to halve the number of baseband (BB) inductors, which each of them is later implemented with a differential gyrator and a capacitor. In the presence of strong blockers at far-out frequencies, a large voltage swing appears at the source terminal of the switches, disrupting the PF operation due to switch failures. Consequently, M shunt capacitors (C_B) are added at those nodes to further attenuate the far-out blockers, thus improving the OOB B_{1dB} by ~3dB.

Fig.3(a) shows the proposed RX block diagram in which the PF first suppresses the blockers and LNTA converts the filtered input voltage to a current, which is then down-converted by passive mixers driven with 8-phase non-overlapping clocks. The TIAs in Fig.3(b) employ a 3rd-order high-pass filter as their feedback impedance to convert the BB currents to voltages and further filter the OOB blockers. The TIA's BB inductors are realized as in the PF. Finally, the harmonic rejection is implemented by a weighted combination of the TIAs' outputs.

Due to the $G_{M,P}$ delay, the RX frequency response suffers from a slight center frequency shift and a few dB of peaking near the lower edge of the passband, as shown in Fig.3(c, e). This delay introduces an undesired feedback current injected into the RX input, which effectively changes Z_{IN} at the passband edges in opposite directions.

To resolve that, we inserted a translational feedback (TF) path by up-converting BB signals at TIAs outputs with 90° phase shift ($\times$ j) and feeding them back to the RX input via R_m resistors and C_m capacitor. As shown in Fig.3(d, e), the TF creates peaking at the passband's upper edge and shifts the RX transfer function to higher frequencies with an offset related to

Die micrograph.

the RX bandwidth (BW_{RF}) and $\omega_{LO}R_mC_m$. Therefore, a flat IB gain can be achieved as the effects of two impedance peakings due to the $G_{M,P}$ delay and TF cancel out each other. Note that R_m value is determined by the 50Ω matching and C_m is chosen to achieve a flat IB gain. In the low-noise mode, where the PF is off, the RX characteristics are different, and thus, another TF path with a different LO phase relation is used to keep the passband gain flat.

The 40nm RX prototype occupies a core area of 0.8mm^2. As shown in Fig.4(a,b), the measured in-band S_{11} and RX gain (G_{RX}) are respectively better than -19dB and 33.5dB over the 0.5-to-3GHz input frequency range. To demonstrate the PF impact on Z_{IN}, S_{11} is measured in Fig.4(c) while sweeping $G_{M,P}$. OOB S_{11} increases with $G_{M,P}$ and reaches -4.5dB. The NF measures down to 2.6dB (3.1dB) at 0.5GHz, and up to 3.9dB (4.7dB) at 3GHz in the low-noise (linear) mode (Fig.4(d)). Fig.4(e) shows the G_{RX} transfer function in three different scenarios. First, the PF and BB inductors in TIAs are disabled. Hence, the system just relies on the single real pole of the TIAs, showing only ~20dB/dec roll-off. In the 2nd case, by enabling the BB inductors in the TIAs, the 3rd-order LPFs with complex poles are activated. Hence, the passband is flattened and the G_{RX} roll-off increases to ~60dB/dec. Finally, activating PF realizes another 3rd-order filtering and increases the G_{RX} transition roll-off to ~120dB/dec. When the frequency exceeds the gyrators' BW, the slope of the transition band returns to ~20dB/dec. As shown in Fig.4(f), when the PF is on (off) and the TF is disabled (enabled), a gain peaking at the lower (upper) edge of the passband is observed. When both blocks are activated, they cancel each other and the IB gain ripple is <0.5dB.

As shown in Fig.5(a,b), thanks to the RX 6th-order channel selectivity, IIP_3/IIP_2 improves from -13/+18dBm IB to +18.7/+77dBm OOB at the adjacent channel, $\Delta f/BW_{RF}$=1, where Δf is the frequency offset from the LO. As depicted in Fig.5(c,d), B_{1dB} improves from -5dBm to +5.5dBm by activating the PF, and NF only degrades by 5dB when RX faces a +5dBm blocker at $\Delta f/BW_{RF}$=3.3. Fig.5(e) shows the measured EVM of a 100MS/s 64QAM OFDM signal with a 10dB PAPR versus its power (P_s). Thermal noise dominates EVM at P_s<-50dBm, the LO phase noise then kicks in and saturates the EVM to -34dB, and finally, EVM degrades due to the RX IB linearity at P_s>-35dBm. With the same input signal at P_s=-60dBm, the RX EVM is only degraded by 2dB when facing a 0dBm blocker at $\Delta f/BW_{RF}$=3.3.

As shown in the comparison table in Fig.6, this work outperforms other LNTA-based RXs [3]-[5] in filtering order, OOB IIP_3 and B_{1dB}, while showing a competitive NF in the low-noise mode. Compared to mixer-first [1][2] and filtering-by-aliasing [6] RXs, only [6] offers a better OOB IIP_3 but at much higher NF, and lower BW, and operating frequency while its passband is not flat.

References:

[1] G. Pini *et al.*, "Analysis and design of a 260-MHz RF bandwidth +22-dBm OOB-IIP3 mixer-first receiver with third-order current-mode filtering TIA," *JSSC*, July 2020.

[2] S. Krishnamurthy *et al.*, "An enhanced mixer-first receiver with distortion cancellation, achieving -80dB/decade RF selectivity and +8-dBm B1dB for adjacent channel blockers," *SSCL*, vol. 4, 2021.

[3] H. Wang *et al.*, "An LO leakage suppression technique for blocker-tolerant wideband receivers with high-Q selectivity at RF input," *JSSC*, June 2021.

[4] H. Razavi *et al.*, "A 0.4-6 GHz receiver for LTE and WiFi," *Symp. VLSI Circuits*, 2021.

[5] M. A. Montazerolghaem *et al.*, "A 3dB-NF 160MHz-RF-BW blocker-tolerant receiver with third-order filtering for 5G NR applications," *ISSCC,* Feb 2021.

[6] S. Bu *et al.*, "A dual-channel high-linearity filtering-by-aliasing receiver front-end supporting carrier aggregation," *JSSC*, Dec 2021.
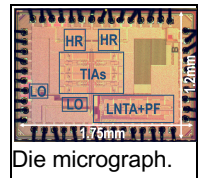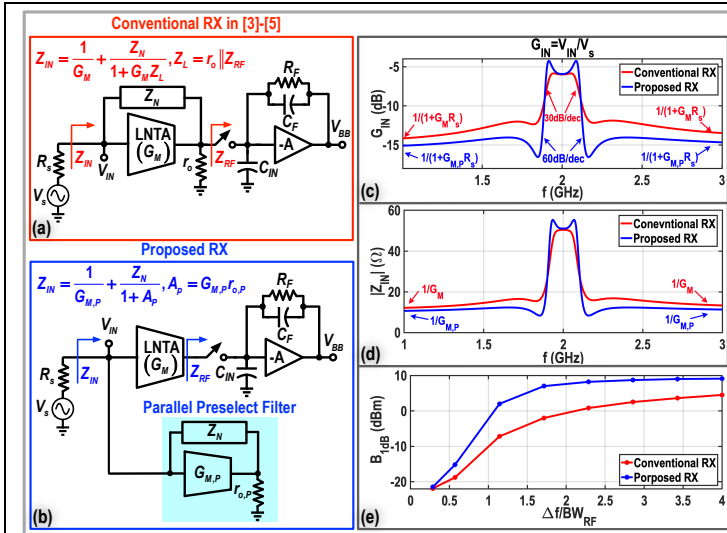
Fig. 1. (a) Conventional LNTA-based RXs [3]-[5] and (b) proposed RX with a PF; the simulation results of (c) G_{IN}, (d) Z_{IN}, and (e) B_{1dB} of those structures when Z_N is an ideal 3rd-order bandstop filter.
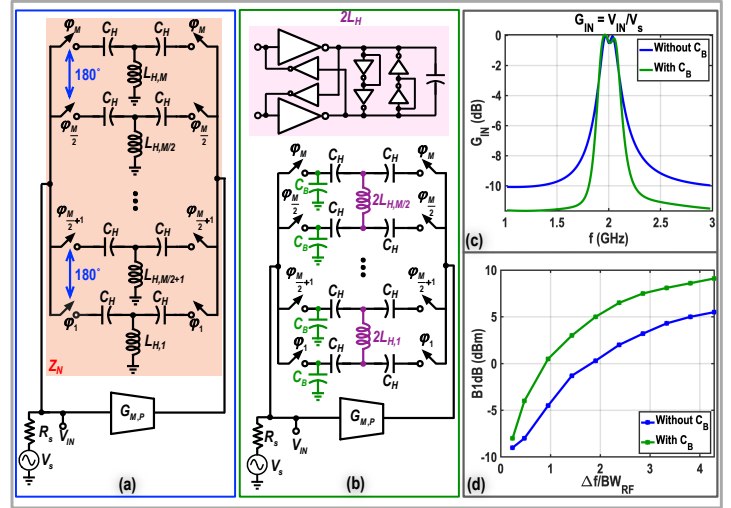

Fig. 2. (a) Initial and (b) final implementation of the preselect filter employing passive mixers and 3rd-order high pass filters; Simulated (c) G_{IN} and (d) B_{1dB} of the proposed structure with/without C_B.
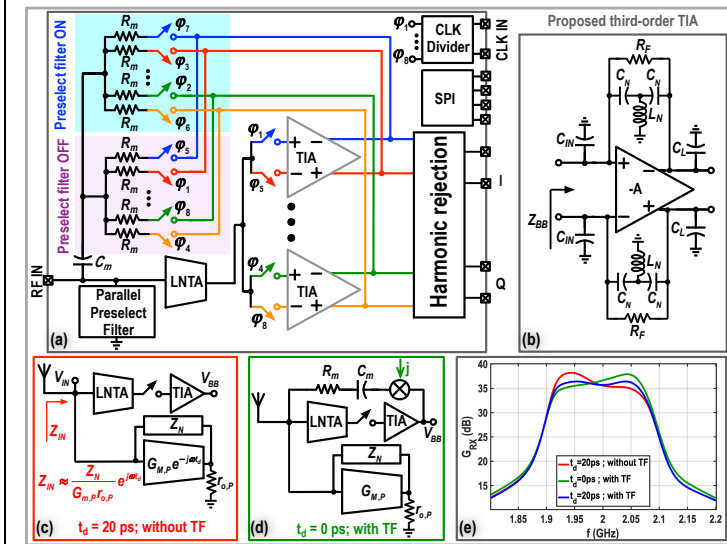

Fig. 3. Block diagram of the proposed (a) RX and (b) 3rd-order TIA; (c) effect of the $G_{M,P}$ delay on Z_{IN}, (d) proposed translational feedback path, and (e) simulated G_{RX} in different scenarios.
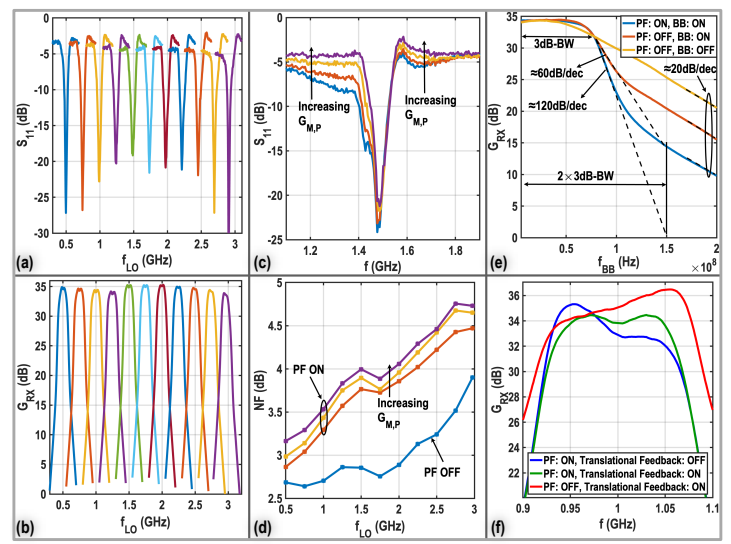

Fig. 4. Measured (a) S_{11} and (b) G_{RX} versus LO frequency; Effect of the PF on (c) S_{11} and (d) NF; Measured gain transfer function (e) and passband response of the receiver in different scenarios (f).
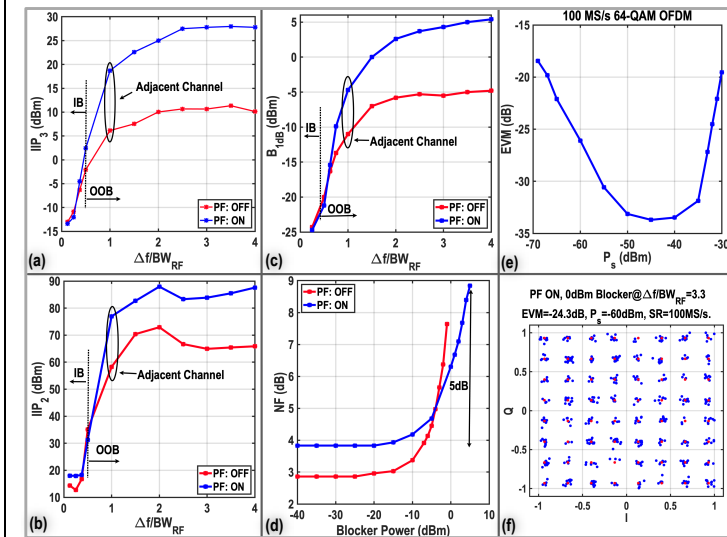

Fig. 5. Measured (a) IIP3, (b) IIP2, (c) B_{1dB}, (d) blocker NF when the PF is OFF/ON; (e) Measured EVM versus input signal power, (d) Measured EVM when facing a 0dBm blocker at $\Delta f/BW_{RF}$=3.3.

	This Work		Wang JSSC 2021[3]	Razavi VLSI 2021[4]	Montazerolghaem ISSCC2021[5]	Pini JSSC2020[1]	Krishnamurthy SSCL2021[2]	Bu JSSC2021[6]
	Low Noise	Linear						
Architecture	LNTA Based		LNTA Based	LNTA Based	LNTA Based	Mixer First	Mixer First	Slice-Based
Technique	Preselect filter and third order TIA		Gm boosting N-path filter	Harmonic rejecting	Programmable zeros and second-order TIA	Third Order Current Mode Filtering	High Order Impedance + N-Path	Filter by Aliasing
Technology	40 nm CMOS		45 nm FDSOI	28 nm	40nm CMOS	28 nm CMOS	28 nm CMOS	28 nm
f_{RF} (GHz)	0.5 - 3		0.2 - 2	0.4 - 6	0.4 - 3.2	0.5 - 3	0.2 - 3.5	0.1 - 1
Gain (dB)	25-45		40	54	36	32.4	16.3	10
Flat BW	Yes		No	No	Yes	Yes	Yes	No
Single Ended Input	Yes		Yes	Yes	Yes	No	Yes	Yes
Supply (V)	1.3		1.2/1.6	-	1.3/1.2	1.8/1.2	1.4/1.2	0.9
Active Area (mm²)	0.8		1.05	1.9	0.6	0.16	1.5	1.3
NF (dB)	2.6 - 3.9	3.1 - 4.7	2.1-2.5	2.11/4.2§	2.7 - 3.6	5.5£	6.5 - 12	10.8
0dBm BNF (dB)	N/A	6.5 $\Delta f/BW_{RF}$ = 3.3	6.7 $\Delta f/BW_{RF}$ = 4	5.3†/7,1§	8.4 $\Delta f/BW_{RF}$ = 3.1	10 $\Delta f/BW_{RF}$ = 4	9 $\Delta f/BW_{RF}$ = 3.1	14 $\Delta f/BW_{RF}$ = 6
BW_{RF} (MHz)	180		20	0.2 - 160	160	260	30	5 - 20
Filtering-order (dB/dec)	-60	-120	-40	-60	-60	-60	-80	-60¥
RF Selectivity (dB/dec)	N/A	-60	-20	-20	-20	-20	-80	N/A
OOB IIP3 (dBm)	7.5 $\Delta f/BW_{RF}$ = 1.5	22.6 $\Delta f/BW_{RF}$ = 1.5	5 $\Delta f/BW_{RF}$ = 1.5	9.4 $\Delta f/BW_{RF}$ = N/A	10 $\Delta f/BW_{RF}$ = 1.5	21 $\Delta f/BW_{RF}$ = 1.5	23 $\Delta f/BW_{RF}$ = 1.5	30 $\Delta f/BW_{RF}$ = 1.5
OOB IIP2 (dBm)	70.4 $\Delta f/BW_{RF}$ = 1.5	82.7 $\Delta f/BW_{RF}$ = 1.5	48 $\Delta f/BW_{RF}$ = 1.5	N/A	50 $\Delta f/BW_{RF}$ = 1.5	70 $\Delta f/BW_{RF}$ = 1.5	N/A	82 $\Delta f/BW_{RF}$ = 8
B_{1dB}(dBm)	-5 $\Delta f/BW_{RF}$ = 3.5	5 $\Delta f/BW_{RF}$ = 3.5	N/A	N/A	-5 $\Delta f/BW_{RF}$ = 2.5	3 $\Delta f/BW_{RF}$ = 3	10 $\Delta f/BW_{RF}$ = 2	12.1 $\Delta f/BW_{RF}$ = 4
LO Leakage (dBm) at 1GHz	-90	-76	-85	N/A	-77	N/A	N/A	-85
EVM (dB)	-27.6‡	-26.3‡	N/A	-25.3¢	-26,4§	N/A	N/A	N/A
0dBm Blocker EVM (dB)	N/A	-24.3‡ $\Delta f/BW_{RF}$ = 3.3	N/A	N/A	N/A	N/A	N/A	N/A
Power (mW)	74 +17mW/GHz	96 +25mW/GHz	68-95	23 - 49	58,5 +17.6 mW/GHz	21,6 + 7.8 mW/GHz	100 mW at 1GHz	21 – 31 /Channel

†Low noise mode, § Harmonic reject mode, £ loss of input balun excluded, ¥ Estimated from figure, ‡ -60dBm 100MS/s 64QAM OFDM, Š -60dBm 140MS/s 64QAM OFDM, ¢ -57dBm 80MS/s 256QAM.

Fig. 6. Performance comparison with state-of-the-art receivers.